Stochastic Cooling Pickup/Kicker Developments for the High-Precision Spectrometer Ring in the HIAF Project at IMP

Guangyu Zhu, Junxia Wu, Fritz Caspers, *Life Fellow, IEEE,* Ze Du, Yuan Wei, Jiancheng Yang, Xuejing Hu, Yong Zhang, Hongming Xie, Long Jing, Zhixue Li, Xin Zhang, Jun Meng, and Jiawen Xia

***Abstract*— Stochastic cooling of the spectrometer ring (SRing) at the High Intensity Heavy-Ion Accelerator Facility (HIAF) project in China, which is used mainly for experiments with radioactive fragment beams, is applied to speed up the cooling process of a stored ion beam. In this study, both a Faltin traveling wave structure and a novel slot-ring standing wave structure based on a ceramic vacuum chamber are discussed and evaluated for the pickup/kicker of the SRing stochastic cooling system. The slot-ring structure should significantly improve the shunt impedance due to the Cherenkov effect. For the Faltin-type structure, the results for the pickup shunt impedance obtained from simulations and from beam measurements agree well. Good agreement is also found between the simulated and measured results for the pickup shunt impedance of the slot-ring structure. Cooling process simulations using the Fokker–Planck equation based on the shunt impedance results for the Faltin- and slot-ring-type pickups are also presented.**

***Index Terms*— Ceramic chamber, pickup/kicker, shunt impedance, spectrometer ring (SRing), stochastic cooling.**

I. Introduction

THE High Intensity Heavy-Ion Accelerator Facility (HIAF) project was proposed by the Institute of Modern Physics (IMP) of the Chinese Academy of Sciences (CAS) in 2009. It will provide high-intensity, high-quality, and high-energy beams, especially of neutron-rich nuclei far from beta-stability, for studies of the nuclear structure of exotic nuclei, nucleosynthesis paths in nuclear astrophysics, nuclear fusion mechanisms, atomic physics, and various areas of applied sciences [1], [2]. The HIAF project was approved in December 2015, and construction started in December 2018. The first beam is expected in December 2024. As an essential part of HIAF, the spectrometer ring (SRing) is designed to perform nuclear mass spectrometry in combination with fast beam cooling [3].

Stochastic cooling is the damping of transverse betatron oscillations and longitudinal momentum spread or synchrotron oscillations of a particle beam by a feedback system. A pick-up electrode (sensor) detects the transverse positions or momenta and longitudinal momentum deviation of particles in a storage ring, and the signal produced is amplified and applied downstream to a kicker electrode, which produces electromagnetic (EM) fields that deflect the particles, in general, in all three directions. In order to act on the particles with their proper corrections, the cooling system must be arranged in such a way that the time delay of the signals in the electronic components matches the transit time of the particles between the pickup and the kicker [4]. The pickup/kickers must be designed to provide the highest possible shunt impedance seen by the beam while maintaining the desired bandwidth [5], [6].

Stochastic cooling of the SRing, which is used mainly for experiments with radioactive fragment beams, is applied to speed up the cooling process of the stored ion beam, which has an initial energy of 400 MeV/u and a momentum a spread of $\Delta p/p = \pm 1.5 \times 10^{-2}$. In the future HIAF phase II upgrade project, the energy of the stochastic cooling system may reach 740 MeV/u. Therefore, in order to consider the redundancy of the SRing stochastic cooling system, we cover the energy range from 400 MeV/u, which is highest priority, to 740 MeV/u in this article. The strategy is to optimize the maximum shunt impedance at 400 MeV/u and ensure that the SRing stochastic cooling system also works at 740 MeV/u. The major beam parameters for stochastic cooling of the SRing are shown in Table I. The radio-isotope (RI) beams from the HIAF fragmentation separator (HFRS) after the production target will have a large momentum spread. If stochastic cooling is used for such beams, the operating frequency of the stochastic cooling system should be small to ensure a large acceptance. However, bunch rotation has been used to decrease the initial momentum spread to $\pm 4.0 \times 10^{-3}$. The time-of-flight (TOF) stochastic cooling method [7] will therefore be used as a first step to precool the stored ion beams because this method has a relatively large momentum acceptance. Then, notch filter cooling [8] will subsequently be applied to attain a lower longitudinal momentum spread. Stochastic cooling will be performed to reduce the transverse emittance to less than

Manuscript received October 14, 2020; accepted November 12, 2020. Date of publication November 19, 2020; date of current version January 19, 2021. This work was supported by the Guangdong Innovative and Entrepreneurial Research Team Program under Grant 2016ZT06G373.

Guangyu Zhu, Junxia Wu, Ze Du, Yuan Wei, Jiancheng Yang, Xuejing Hu, Yong Zhang, Hongming Xie, Long Jing, Zhixue Li, Xin Zhang, Jun Meng, and Jiawen Xia are with the Department of Accelerator Technology Center, Institute of Modern Physics, Chinese Academy of Science, Lanzhou 730000, China, and also with the School of Nuclear Science and Technology, University of Chinese Academy of Sciences, Beijing 100049, China (e-mail: wujx@impcas.ac.cn).

Fritz Caspers is with CERN, 1211 Geneva, Switzerland.

Color versions of one or more figures in this article are available at https://doi.org/10.1109/TNS.2020.3038525.

Digital Object Identifier 10.1109/TNS.2020.3038525

TABLE I
MAJOR BEAM PARAMETERS FOR STOCHASTIC COOLING OF THE SRING

Circumference (m)	277.3
Magnetic rigidity (Tm)	1.5-15
Operation modes	Normal
Ion species	Rare Isotope Beams (RIBs)
Intensity (ppp)	10^3-10^8
Beam structure	Coasting beam (DC-beam)

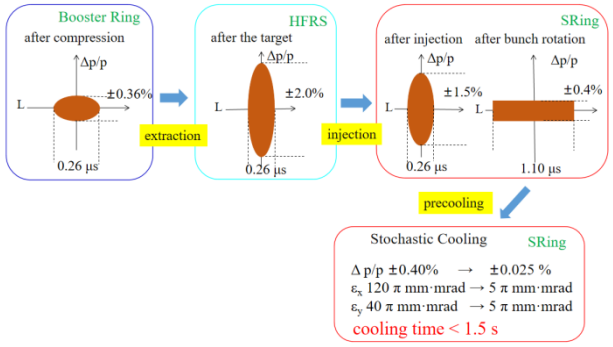

Fig. 1. Cooling operation on the SRing. All momentum spread ($\Delta p/p$) and emittance ($\varepsilon_x/\varepsilon_y$) values are $\pm 2\sigma$ values. The cooling time of stochastic cooling is required to be less than 1.5 s.

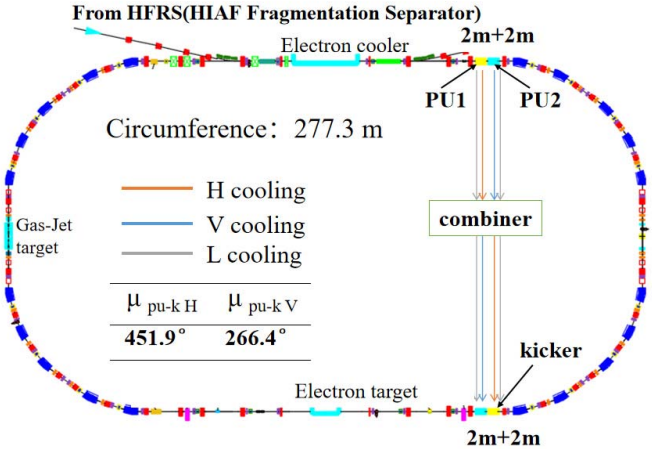

Fig. 2. Layout of the stochastic cooling system on the SRing. H: horizontal, V: vertical, L: longitudinal, PU1: pickup1 of stochastic cooling system for H + L plane, PU2: pickup2 of stochastic cooling system for V + L plane, $\mu_{\text{pu-kH}}$: the horizontal betatron phase advance from the pickup to the kicker, $\mu_{\text{pu-kV}}$: the vertical betatron phase advance from the pickup to the kicker. The blue, red, and purple squares represent the dipoles, quadrupoles, and sextupole magnets, respectively.

5π mm mrad, and a $\Delta p/p$ of $\pm 4.0 \times 10^{-3}$ to $\pm 2.5 \times 10^{-4}$ within 1.5 s for the RI beams, as shown in Fig. 1. Fig. 2 shows the layout of the SRing stochastic cooling system. Here the space is reserved in advance for SRing stochastic cooling, with 4 m for the pickups and 4 m for the kickers.

The pickups and kickers are in straight sections, without dispersion. It is planned to have two pickup tanks and two kicker tanks, which can perform both transverse and longitudinal cooling. The betatron phase advance from the pickup to kicker is approximately $90° + k\pi$ $(k = 0, 1, 2, \ldots)$ for both horizontal and vertical cooling.

The first pickup/kickers used in the Antiproton source at Fermilab were 3-D stripline-type devices that were developed at Lawrence Berkeley National Laboratory (LBNL) in the early 1980s [9], [10]. While these arrays proved worthy as the initial antennas, they were difficult and costly to manufacture. They also suffered from mechanical failures where a kicker loop antenna on several occasions would become unsoldered due to heat dissipation and fall into the beam aperture. The electrode of the pickups and kickers of stochastic cooling in CERN antiproton decelerator (AD) acts like a quarter-wave directional coupler [11], [12]. In order to improve the signal-to-noise ratio and the transverse cooling efficiency of AD stochastic cooling, a cryogenic tank and movable mechanic structure are used. The pickups and kickers of stochastic cooling in CERN AD have operated more than 20 years since 1998. However, the AD structure is mechanically complex, costly, and difficult to maintain. The pickups and kickers of stochastic cooling for COSY in Jülich are very similar to the structure of AD/AC [13]. Therefore, it is necessary to develop new pickups/kickers more suitable for the HIAF stochastic cooling system. A novel slot-ring standing wave structure based on a ceramic vacuum chamber and a Faltin traveling wave structure are discussed and evaluated for the pickup/kicker of the SRing stochastic cooling system to reduce the manufacturing cost, reduce the difficulty, shorten the production cycle, and improve efficiency.

The organization of the article is as follows. Section II is devoted to express the choice of operating bandwidth of the SRing stochastic cooling system. In Section III, the shunt impedance of the pickup and the kicker is explained. Then, the design of both a Faltin-type and slot-ring-type pickup/kicker using the High Frequency Structure Simulation (HFSS) software is illustrated. Next, the pickup shunt impedance measurements for both the Faltin and slot-ring prototypes are given. In Section IV, the simulation calculation results of the cooling process are given. The summary and the concluding remarks are given in Section V.

II. CHOICE OF OPERATING BANDWIDTH

For longitudinal cooling, the synchronization error due to undesired mixing between the pickup and the kicker is due to a timing error relative to the reference particle [14], [15]

$$\frac{\delta T}{T_{p\to k}} = -\eta \frac{\Delta p}{p} + \alpha_p \frac{\delta\left(\frac{m}{q}\right)}{\left(\frac{m}{q}\right)}. \tag{1}$$

For different beams with different mass-to-charge ratios, m/q, $T_{p\to k}$ denotes the time of flight from the pickup to the kicker, α_p is the momentum compaction from the pickup to the kicker, and $\eta = \gamma^{-2} - \alpha_p$ is the frequency slip factor. In the case of a single beam, the second term in the formula is zero. The longitudinal TOF cooling force scales as

$$F_{\parallel} \propto \sum_n G \cdot \sin\left(n\omega_0 T_{p\to k}\eta \frac{\Delta p}{p}\right). \tag{2}$$

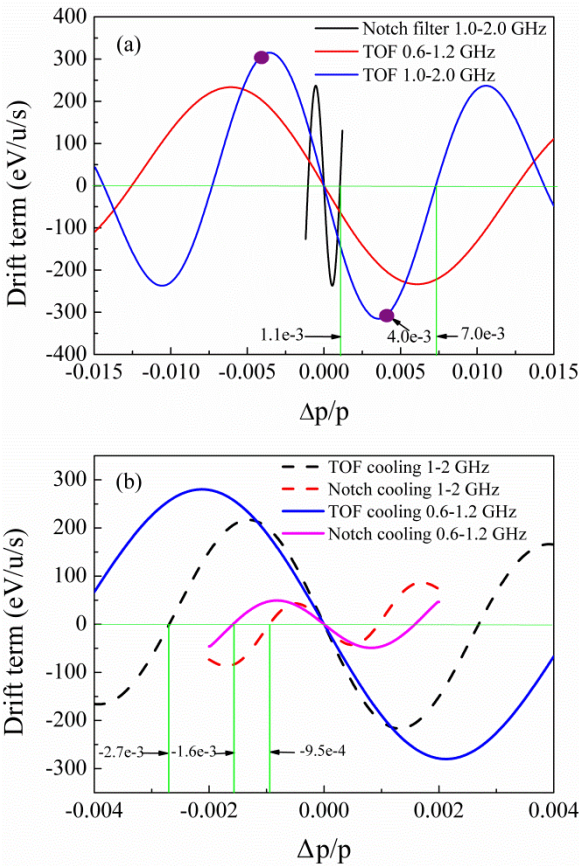

Fig. 3. Cooling force as a function of momentum spread for the SRing TOF cooling and notch filter cooling: (a) energy = 740 MeV/u and (b) energy = 400 MeV/u.

If the system is tuned to the reference particle, G includes the transmission gain from the pickup to the kicker, the frequency response of the pickups and kickers, and n is the harmonic number. This is expressed as the sum of the harmonics of the revolution frequency inside the cooling bandwidth. It can be clearly seen that for a momentum spread that is too large, the cooling force changes sign, that is, it heats up the beam. Fig. 3(a) shows the acceptance for the TOF and notch filter cooling for an energy of 740 MeV/u and a bandwidth of 1–2 GHz. The two markers on the blue curve indicate a momentum dispersion of ±0.4%. Fig. 3(b) shows the acceptance for the TOF and notch filter cooling for an energy of 400 MeV/u. According to the cooling force simulation results, we can see that:

1) For the pink solid curve, the notch filter requires a much tighter momentum spread and cannot accept $|\delta(p)/p| > 0.0016$.
2) The blue solid curve does not changes sign when $|\delta(p)/p)| \leq 0.004$. This means that TOF 0.6–1.2 GHz cooling will work to cool the beam momentum spread of 0.004.
3) The black dotted curve changes sign outside $|\delta(p)/p)| = 0.0027$. This means that the acceptance of TOF cooling is smaller than the beam momentum spread ($|\delta(p)/p)| = 0.004$) if the cooling bandwidth is 1–2 GHz.

Therefore, we changed the operating bandwidth to 0.6–1.2 GHz where the beam spread fits inside the acceptance of the TOF cooling system when the energy is 400 MeV.

III. Pickup/Kicker

The behavior of an electrode system when it functions as a pickup is intimately related to its behavior as a kicker due to the reciprocity between the kicker and the pickup. In analyzing the behavior of an electrode system, it frequently proves easier to calculate its performance as a kicker, that is, the response of the beam when the structure is powered externally, than its performance as a pickup, where a boundary-value problem must be solved, with the beam current as a source term [16]. In this study, a power of 1 W is input into the kicker and the accelerating voltage is determined by integrating the electric field along a particle trajectory above the slots. The input power and beam voltage then yield the kicker shunt impedance, which is then converted into pickup shunt impedance (modified by a factor of 1/4). The shunt impedance is the true efficiency of the kicker, which depends on the nature of the electrodes themselves and not on the impedance of the input cable. The longitudinal constant $K_{\parallel}$, shunt impedance $Z_{\parallel(kic\,\mathrm{ker})}$, and pickup shunt impedance $Z_{\parallel(\mathrm{pick\text{-}up})}$ are given by Goldberg and Lambertson [17]

$$K_{\parallel} = \frac{V}{V_k} \tag{3}$$

$$V = \int_a^b E_z e^{jk_B z} dz \tag{4}$$

$$Z_{\parallel(\mathrm{kic\,ker})} = Z_{\parallel} T^2 = \frac{\left|V^2\right|}{2P_k} = Z_c \left|K_{\parallel}\right|^2 \tag{5}$$

$$Z_{\parallel(\mathrm{pick\text{-}up})} = \frac{P_{pu}}{I_b^2} = \frac{1}{4} Z_{\parallel(\mathrm{kicker})} \tag{6}$$

where V is the accelerating/decelerating voltage acting on the beam, E_z is accelerating field, and k_B is the beam wavenumber $k_B = \omega/\beta c$. V_k is the input voltage on the power coupler, T is the transit-time factor, $K_{\parallel}$ is calculated from the (longitudinal electric) fields, which are generated when the plates are excited with equal voltages of the same sign, P_k is the power into the kicker, P_{pu} is the power from the pickup, and I_b is the beam current.

The transverse kicker constant $\vec{K}_{\perp}$, transverse shunt impedance $Z_{\perp(kic\,\mathrm{ker})}$, and transverse pickup transfer impedance Zp are given by

$$\vec{K}_{\perp} = -\frac{1}{jk_{\mathrm{B}}} \nabla_{\perp} K'_{\parallel} \tag{7}$$

$$Z_{\perp(\mathrm{kic\,ker})} = Z_{\perp} T^2 = Z_c \left|\vec{K}_{\perp}\right|^2 \tag{8}$$

$$Z_p = k_B \sqrt{Z_c Z_{\perp} T^2}/2 \tag{9}$$

where $K'_{\parallel}$ are excited with equal voltages of the opposite sign, Z_c is the characteristic impedance of the input line, and $k_B = \omega/\beta c$.

The horizontal and vertical beam apertures of the pickup and the kicker are 200 and 120 mm, respectively. In the future HIAF phase II upgrade project, the beam pipe diameter of the

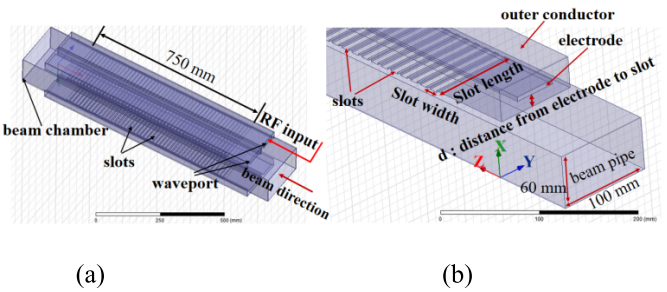

Fig. 4. Dimension of the Faltin traveling wave-type kicker prototype, with a slot length and width of 10 and 90 mm, respectively. The slot cell length is 15 mm. (a) 3-D diagram with 0.75-m-long rails. (b) Quarter partial HFSS model of Faltin structure, the beam is traveling along the z-direction.

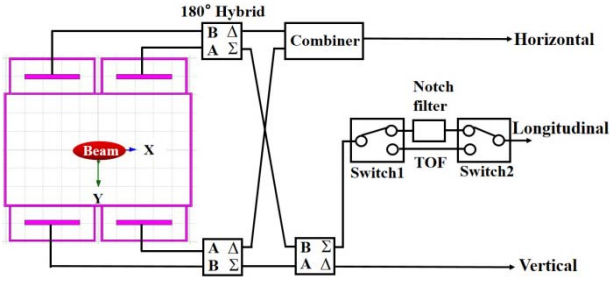

Fig. 5. Stochastic cooling system, with a Faltin-type pickup, including both TOF and notch filter methods in the SRing, and showing the combination of signals in the sum and differential modes. Note that 180° hybrids are ideal for performing summation/differential combining. However, the combiner is ideal for performing in-phase combining.

SRing will be 118 mm. Both a Faltin traveling wave structure and slot-ring standing wave structure were considered for the pickup/kicker of the SRing stochastic cooling system. The commercial simulation software ANSYS HFSS [18] was used for the longitudinal and transverse numerical simulations.

A. Faltin Structure

1) Simulation and Optimization for the Faltin Structure: The Faltin electrode [19], which is used due to its low number of feedthroughs, robustness, and ease of manufacture, is a rectangular coaxial waveguide, with slots that couple to the beam. For the traveling wave-type kicker, it is crucial that the phase velocity in the waveguide be approximately equal to the particle velocity across the desired frequency band of operation. In a momentum cooling system, the pickup signals are combined in the sum mode and similarly, the signal to the kicker electrodes is also applied in the sum mode, providing longitudinal fields to accelerate or decelerate the passing particles. Betatron or transverse cooling systems use pickups in differential mode to generate the beam error signal, and then the kickers apply a transverse field to the particles by applying the error signal to the kicker electrodes in a "push-pull" fashion. Fig. 4 is a diagram of a section of the pickup/kicker structure containing four Faltin rails intended for horizontal and vertical difference measurements. The total length of the rails is 750 mm and d is the distance from the electrode to the slot. Fig. 5 shows how the signals at the Faltin-type pickup are combined to extract horizontal error signals and the combined vertical and longitudinal error signals.

A power of 1 W is input into the kicker in sum mode and the accelerating voltage is found by integrating the electric field (located at $x = 0$, $y = 0$) along a particle trajectory with the correct phase advance above the slots. According to (5), the input power and beam voltage then yield the longitudinal kicker shunt impedance. According to the HFSS sweep parameter simulation, the frequency corresponding to the peak of the shunt impedance is mainly determined by the width of the slot, as shown in Fig. 6. We can see that the slot length was varied from 75 to 90 mm and was found to have large influence on the shunt impedance and frequency response. For small slot length, the shunt impedance is smallest over the operating band. However, as the slot length increases, the operating band decreases. Fig. 7 shows the simulated longitudinal kicker shunt

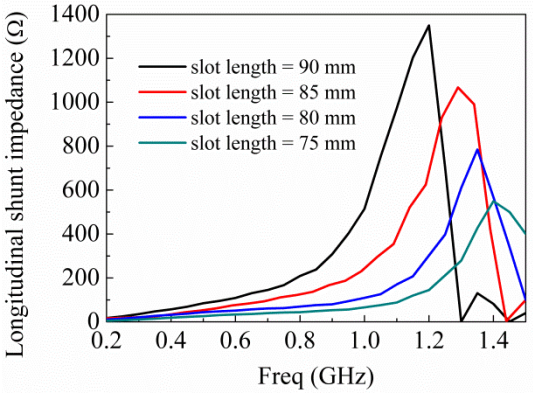

Fig. 6. Longitudinal kicker shunt impedance for a 0.75-m long Faltin structure when varying the slot length, with a slot width of 10 mm and the distance from electrode to slot was $d = 15$ mm.

impedances for different beam energies and different d, which was optimized to 400 MeV/u (beta = 0.71), when the slot length and width is 10 and 90 mm, respectively. We can see clearly that the shunt impedance of the Faltin rail structure is sensitive to the beam velocity beta. Fig. 7 also shows that d is a sensitive parameter of the Faltin kicker for the shunt impedance. When we decrease d, the shunt impedance at a lower frequency, for example, 0.6–0.8 GHz improves; however, the peak value of shunt impedance deteriorates at higher frequencies, for example, when $d = 12$ mm and beta = 0.71; it decreases to 1080 Ω at 1.072 GHz, and even when $d = 9$ mm and beta = 0.71, it decreases to 631 Ω at 0.9 GHz, as shown in Fig. 7(b) and (c). From Fig. 7(a), we can clearly see that the maximum optimized longitudinal kicker shunt impedance of the 0.75 m Faltin structure for beta = 0.71 is 1349 Ω at 1.197 GHz. Table II lists the main optimized dimension of the Faltin rail structure.

In this article, we optimize structures only for longitudinal performance and check whether the resulting transverse performance is still sufficient. A power of 1 W is input into the kicker in the differential mode (in "push-pull" fashion) and the accelerating voltage is found by integrating the electric field (vertical: $x = 0$, $y = 1$ mm; horizontal: $x = 1$ mm, $y = 0$) along a particle trajectory with the correct phase advance above the slots by using HFSS fields calculator. We integrate

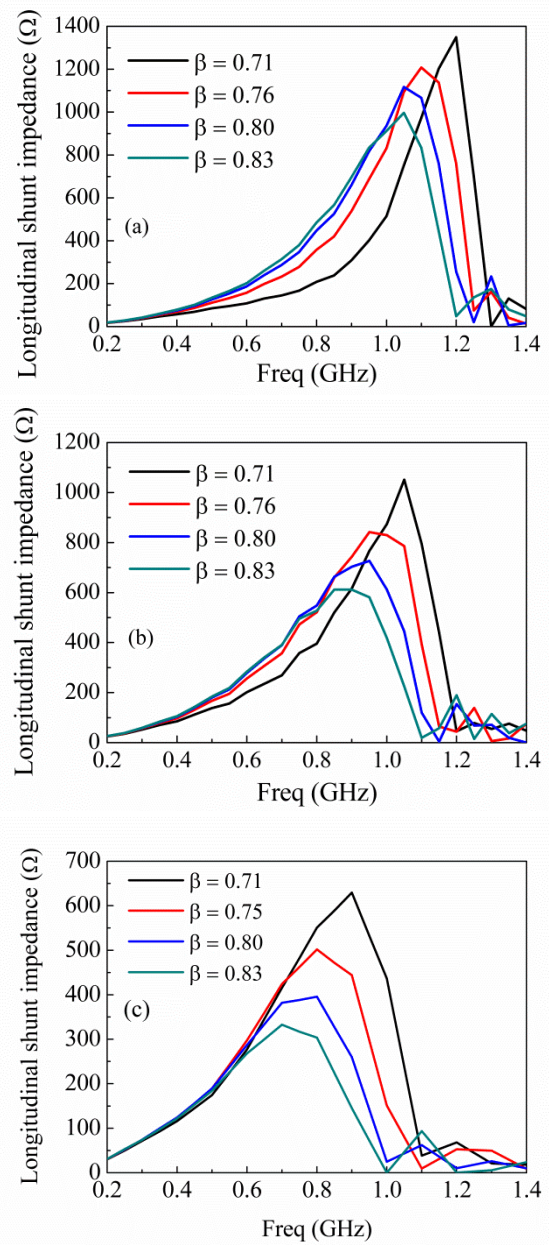

Fig. 7. Longitudinal kicker shunt impedance for a 0.75-m long Faltin structure when the distance from the electrode to the slot was (a) $d = 15$ mm, (b) $d = 12$ mm, and (c) $d = 9$ mm, with a slot length and width of 10 and 90 mm, respectively.

TABLE II
LIST OF THE OPTIMIZED DIMENSION OF FALTIN RAIL STRUCTURE

Structure	Dimension
Slot length	90 mm
Slot width	10 mm
Slot cell length	15 mm
Electrode thickness	5 mm
Electrode width	48 mm
Distance from electrode to slot	15 mm
Outer conductor height	36 mm
Outer conductor width	90 mm

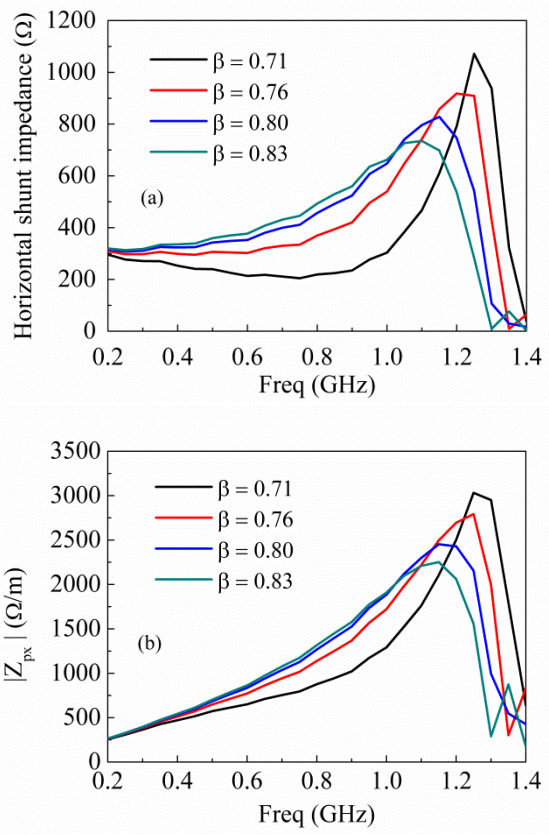

Fig. 8. (a) Horizontal kicker shunt impedance and (b) horizontal pickup transfer impedance.

at the positions (0, 1 mm) and (1, 0 mm), because we can easily calculate the electric field gradient, since E_z is zero at (0, 0 mm). According to (8), the input power and beam voltage then yield the transverse kicker shunt impedance for different beam energies, as shown in Figs. 8(a) and 9(a). We then calculate the pickup transfer impedance according to (9), as shown in Figs. 8(b) and 9(b).

2) Beam Measurement for the Faltin-Type Pickup: To test the initial designs and accuracy of the HFSS, prototypes of the pickup with total slot lengths of 0.75 m were constructed and tested at the Heavy Ion Research Facility in the Lanzhou-Cooler Storage Ring (HIRFL-CSR) [20]. Fig. 10 shows a photograph of a Faltin fabricated prototype. The wave in the pickup induced by the beam traveled parallel to the beam and at the same velocity, such that induction from the beam to the slotted coaxial waveguide through each slot was added constructively. The output signals were picked up from four feedthroughs downstream, another four feedthroughs were loaded by a 50-Ω radio frequency (RF) load upstream. A diagram of the longitudinal pickup shunt impedance measurement setup for the Faltin structure is shown in Fig. 11.

According to the definition given by Goldberg and Lambertson [17], for N particles, with a charge state of q and revolution frequency of f_{rev}, the Schottky power from the pickup signal into an impedance-matched load Zc at each

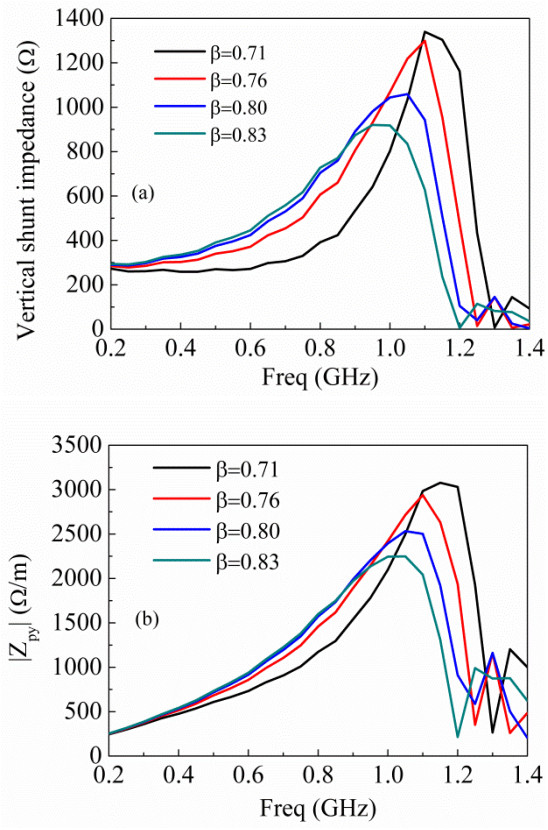

Fig. 9. (a) Vertical kicker shunt impedance and (b) vertical pickup transfer impedance.

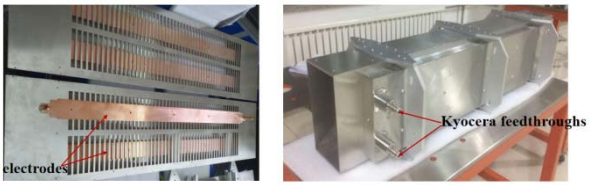

Fig. 10. Photographs of a Faltin prototype structure, with eight Kyocera feedthroughs. (Left) Before assembly. (Right) After assembly.

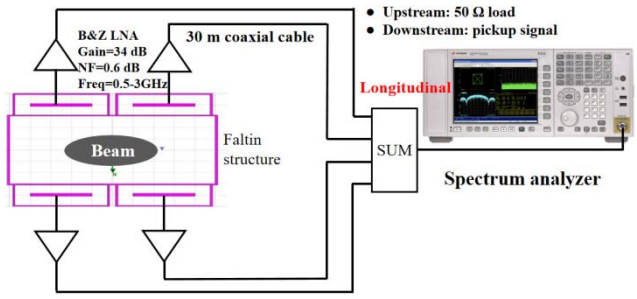

Fig. 11. Diagram of the longitudinal shunt impedance measurement setup for the Faltin structure. The output signals were picked up from four feedthroughs downstream. Four other feedthroughs were loaded by a 50-Ω RF load upstream.

harmonic is

$$P_{\text{sch}} = \left(I^2\right) \cdot Z_{\parallel(\text{pick-up})} = 2N(q\text{ef}_{\text{rev}})^2 \cdot Z_{\parallel(\text{pick-up})} \qquad (10)$$

where $Z_{\parallel(\text{pick-up})}$ is the pickup shunt impedance.

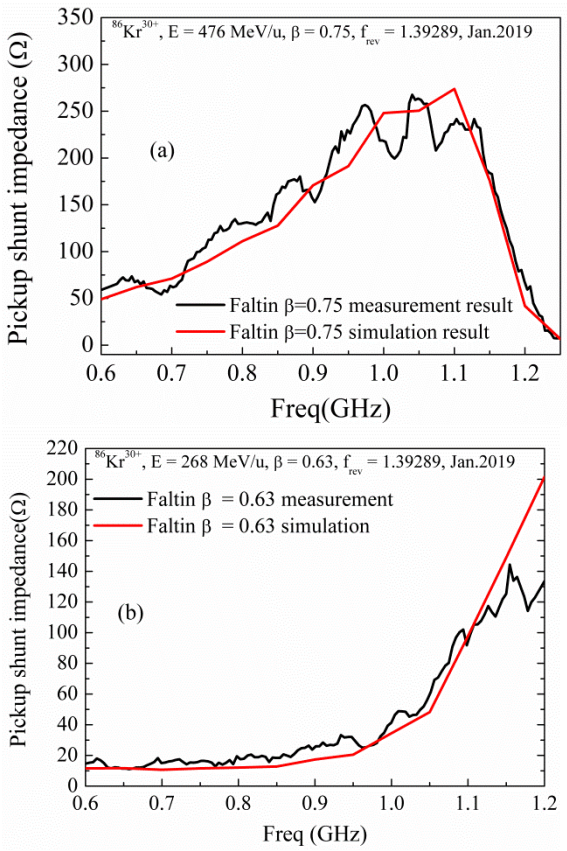

Fig. 12. Comparison of the Faltin longitudinal pickup shunt impedance results from simulation and from beam measurement with a $^{86}Kr^{30+}$ beam: (a) energy = 476 MeV/u and (b) energy = 268 MeV/u. The particle number is approximately 5×10^7. Note that the Faltin-type pickup device itself involves the structure wall loss, amplifier gains, cable loss, circuit loss calibrations, etc. We have considered them and done the calibration benchmarks.

Fig. 12 is a comparison of the results for the pickup shunt impedance from the HFSS simulation and from beam measurement with an $^{86}Kr^{30+}$ beam at energies of 476 and 268 MeV/u. The measured result has some resonances/ripples, as shown in Fig. 12(a), which are mainly caused by the Schottky power estimation error due to randomness of white noise, especially caused by an uncertainty in absolute Schottky power measurements of ±1 dB as well as a beam spectrum uncertainty in the same order of magnitude, and partly caused by the impedance mismatch from Kyocera feedthroughs and adapter of cables which are not considered in the simulation. Fig. 12(b) shows that at higher frequency around at 1.2 GHz, the measured result deviates from the simulation probably because of some interference signal and partly because an uncertainty in absolute Schottky power measurements of ±1 dB. But anyway there is a very good agreement between the simulation and measurement results for the Faltin-type pickup shunt impedance.

B. Slot-Ring Structure

1) Simulation and Optimization of the Slot-Ring: The slot-ring structure, which is a standing wave structure, was proposed originally by Stassen *et al.* [21]. This slot-ring coupler,

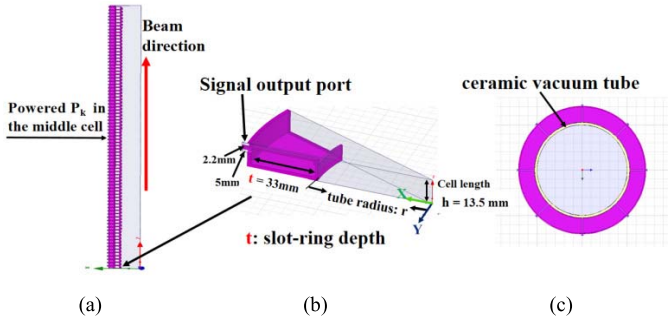

Fig. 13. Kicker shunt impedance simulation model for the slot-ring structure: (a) HFSS model with 64 one-sixteenth cells. (b) Dimensions of a one-sixteenth cell with symmetric boundary, without a ceramic vacuum tube. (c) One slot-ring full cell with an 8-mm thickness ceramic vacuum tube.

with a symmetric arrangement of eight shorted electrodes gives a significantly higher longitudinal impedance than a comparable quarter-wave structure. The total image current passes the surrounding uninterrupted gap formed by two adjacent rings. The round cell is similar to a classical iris loaded linac cell and is heavily loaded with eight 50-Ω coaxial lines to obtain the octave bandwidth. However, the disadvantages of a slot-ring structure directly installed in the vacuum tank are that it is very difficult to remove heat from a kicker when the combiner/divider board is in the vacuum rather than in the air. It also cannot be used for ultrahigh vacuum conditions requiring a 250°–300° high-temperature bake-out. Finally, it is difficult to install and maintain when the slot-ring and combiner/divider board are in the vacuum tank.

We mainly study kicker shunt impedance because, for the HFSS simulation, it is easier to determine the field inside a structure for a given input power level and frequency than to place a beam (simulated by many short current sheets, with phase offsets according to beam velocity and frequency) and then calculate the output signals. The single-cell longitudinal shunt impedance is obtained by powering one of many cells, with $P_k = 1$ W at various frequencies in the working band, and then integrating the longitudinal electrical field experienced by particles traversing the complete structure at these frequencies. The results of the integration are obviously dependent on the frequency, the particle velocity, and the transverse position (X, Y). For this kicker shunt impedance evaluation method to be valid, the fields must have practically vanished before they reach the extremities of the structure. This condition is best obtained by powering a cell situated toward the middle of the structure. Fig. 13(a) shows the HFSS simulation model of a slot-ring structure, with 64 one-sixteenth cells for longitudinal kicker shunt impedance. To take advantage of the symmetry of the structure, we model each ring as a $\pi/8$ wedge. Fig. 13(b) shows the dimensions of a one-sixteenth cell without a ceramic vacuum tube, where t is the slot-ring depth and r is the beam chamber radius (here r is 100 mm as the beam aperture size of the SRing is 200 × 120 mm). Fig. 13(c) shows a one slot-ring full cell model with an 8-mm thickness ceramic vacuum tube. Fig. 14 shows the transverse cut through a slot-ring kicker, with an electric field of one excited middle cell. The longitudinal kicker is excited by the sum mode (all electrodes in phase), as shown in Fig. 14(a). The transverse

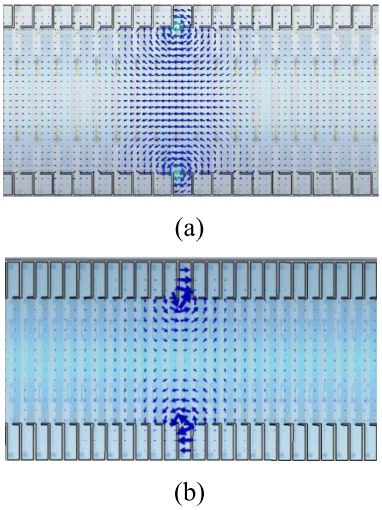

Fig. 14. Electrical field distribution for the slot-ring structure: (a) sum mode, quasi-TM011 mode is excited. (b) Differential mode, quasi-TM111 mode is excited.

kicker is excited by the difference mode (top and bottom electrodes in push-pull fashion), as shown in Fig. 14(b).

In HFSS, we could define the variables what we want. For the slot-ring structure shunt impedance simulation, we define several variables, for example, slot-ring depth t, cell length h, and beam tube radius r. In order to find which parameter has the greatest influence on the shunt impedance, we choose "one at a time sequentially" but not "all at once" to simulate. Through the sweep parameter simulation in the HFSS, we found that the most sensitive parameter is the slot-ring depth t. It defines the additional length for the image current and thus could be used to tune the resonant frequency to the desired band. The cell length h is also sensitive. Slimmer cells have a smaller impedance, but a higher impedance per length. Very slim cells are not advisable, because the combiner boards become more complex. As a tradeoff, we use $h = 13.5$ mm, as for the kicker. The kicker shunt impedance is also dependent on the beam vacuum tube radius r. Fig. 15 shows the simulation results of the longitudinal kicker shunt impedance for a one cell slot-ring structure, without a ceramic vacuum tube, when $t = 33$ mm, $r = 59$, 100 mm, and $h = 13.5$ mm. It also shows that this kind of slot-ring structure is sensitive to the beam velocity beta. When the beam velocity beta increased, the shunt impedance also increases significantly. From Fig. 15, as we expected, as the radius r increases, the shunt impedance decreases. When the radius r increases from 59 to 100 mm, the maximum kicker shunt impedance of the slot-ring reduces from 15.5 Ω at 1.6 GHz to only 3.0 Ω at 1.3 GHz for beta = 0.71. The main reason for this is that the beam is the current source and the electrode acts like the antenna, and hence the farther the antenna is from the time-varying current source, the smaller the signal it receives. In parallel, the resonant frequency shifts from around 1.6 to 1.35 GHz.

As indicated by the analysis in the previous paragraph, the slot-ring structure is more suitable for a high-energy beam (high beta). To improve the shunt impedance for beta = 0.71, we found that if the slot-ring structure is installed outside

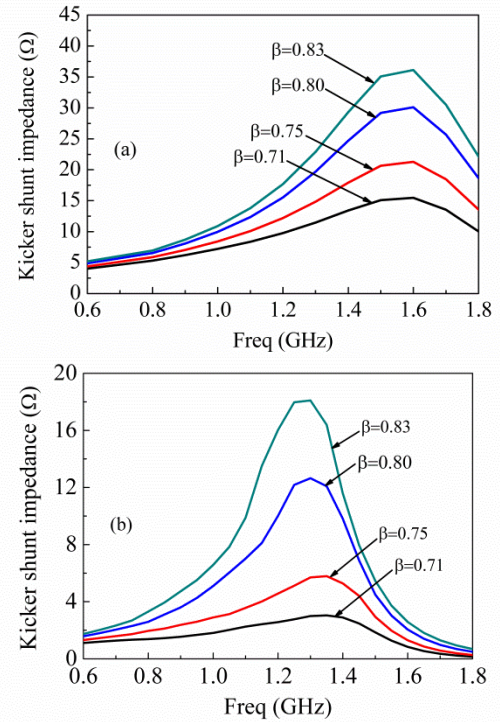

Fig. 15. Longitudinal kicker shunt impedance for a one-cell slot-ring structure, without a ceramic tube, when t = 33 mm and cell length = 13.5 mm: (a) beam tube radius r = 59 mm and (b) beam tube radius r = 100 mm.

a ceramic vacuum chamber, the kicker shunt impedance can be significantly improved through the Cherenkov effect [22]. The main reason is the dielectric sort of "pulls" the EM field closer to the gap of the slot-ring structure. In contrast to normal stripline TEM wave pickups which are also used in traveling as well as standing wave mode where in that case the backward wave interacts with the beam for highly relativistic particles, the Cerenkov pickup is a forward coupler sort of comparable with Faltin-type structures. We see a clear enhancement of the sensitivity from the presence of a dielectric beam pipe close to the slot-ring structures. From Fig. 16, we can see that when the slot-ring depth t increased, the maximum kicker shunt impedance of the slot-ring also increased, and the resonant frequency deceased. The reason is slot-ring-type is a standing wave structure, which likes a quarter wavelength resonance cavity, and the resonant frequency decreases as the size increases. Fig. 17 shows a longitudinal kicker shunt impedance for a one-cell slot-ring structure with an 8-mm thickness ceramic tube, when t = 33 mm and cell length = 13.5 mm. From Fig. 17(a), we can see clearly that the maximum optimized longitudinal kicker shunt impedance of the one-cell slot-ring structure for beta = 0.83 is 53 Ω. By comparing Figs. 15(b) and 17(b), we can see that the kicker shunt impedance of the one slot-ring cell is increased by more than five times, from 3.0 Ω without a ceramic tube to 17.3 Ω with an 8 mm thickness ceramic tube, when the beam tube radius r = 100 mm and beta = 0.71. Even for the beta = 0.83 case, the kicker shunt impedance value of a one slot-ring cell with an 8 mm thickness ceramic tube is doubled. The calculated results are consistent with the theoretical prediction of [22]. It was also found that the resonant frequency $\omega = 1/\sqrt{LC}$ decreases from 1.3 to 0.85 GHz when the introduction of a ceramic vacuum chamber (99% Al_2O_3, εr = 9.8 at 1 GHz and 298 K) increases the capacitance.

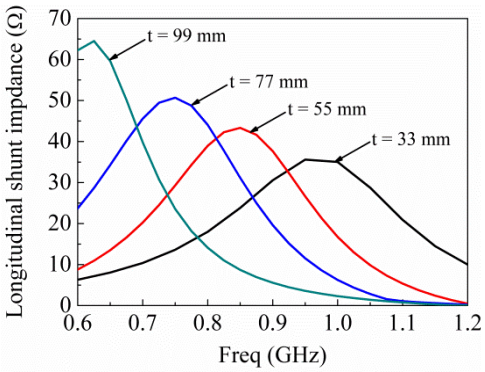

Fig. 16. Longitudinal kicker shunt impedance for a one-cell slot-ring structure with an 8-mm thickness ceramic vacuum tube, where t is the slot-ring depth, when beam tube radius r = 59 mm and β = 0.71. Note that the sweep range of t is from 11 to 99 mm, the sweep step is 11 mm, a total of nine points were swept, only four typical curves are plotted.

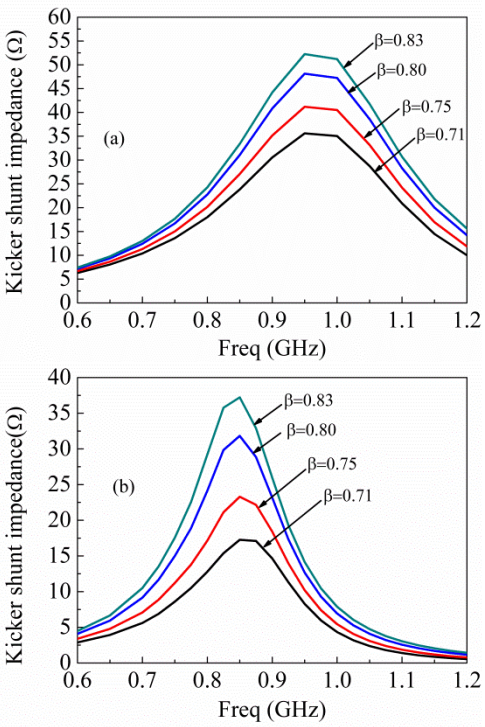

Fig. 17. Longitudinal kicker shunt impedance for a one-cell slot-ring structure with an 8-mm thickness ceramic vacuum tube, when t = 33 mm and cell length = 13.5 mm: (a) beam tube radius r = 59 mm. (b) Beam tube radius r = 100 mm.

By comparison with the same length of Faltin structure, the longitudinal kicker shunt impedance of the 0.75 m long (55 cells) slot-ring structure was calculated for different beta values by multiplying 55 cells when t = 33 mm, beam tube radius r = 100 mm, and one cell length = 13.5 mm with an 8 mm thickness ceramic tube, as shown in Fig. 18. From Fig. 18, the maximum optimized longitudinal kicker shunt impedance of the 0.75 m slot-ring structure for beta = 0.71 was 950 Ω at 0.85 GHz, which is smaller than the value for Faltin structure of 1349 Ω at 1.197 GHz in Fig. 7(a),

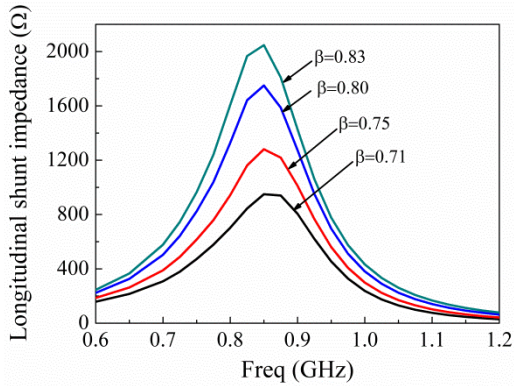

Fig. 18. Longitudinal kicker shunt impedance for a 0.75-m long (55 cells) slot-ring structure when $t = 33$ mm, beam tube radius $r = 100$ mm, and one cell length = 13.5 mm with an 8-mm thickness ceramic tube.

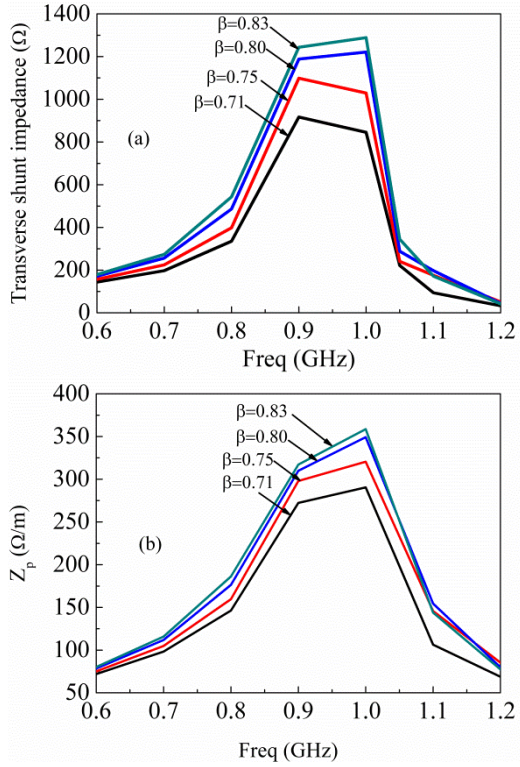

Fig. 19. (a) Transverse kicker shunt impedance for a 0.75-m long (55 cells) slot-ring structure, when $t = 33$ mm, beam tube radius $r = 100$ mm, and one cell length = 13.5 mm with an 8-mm thickness ceramic tube. (b) Transverse pickup transfer impedance for one-cell slot-ring structure, when $t = 33$ mm, beam tube radius $r = 100$ mm, and one cell length = 13.5 mm with an 8-mm thickness ceramic tube.

and the slot-ring structure has a narrower band (from 0.6 to 1.2 GHz). According to (8) and (9), the transverse kicker shunt impedance and transverse pickup transfer impedance for the 0.75 m long (55 cells) slot-ring structure are optimized to 1 GHz, as shown in Fig. 19.

Figs 18 and 19 also show that the maximum longitudinal and transverse impedance have been optimized to between 0.8 and 1.0 GHz, which is exactly what we expected. It is a tradeoff to allow the maximum transverse and longitudinal impedances to approach the central frequency 0.9 GHz of the operating bandwidth.

Fig. 20. Photograph of the 16 slot-ring cells structure, with 16-way Wilkinson stripline combiner boards and an 8-mm thickness ceramic vacuum chamber. The combiner boards consist of two basic elements: the Wilkinson combiners and the unit-delay-lines. The unit-delay-line is simply a piece of microstrip.

Faltin structure has higher shunt impedance, wider bandwidth, and requires fewer feedthroughs, when the beam aperture size of the SRing is 120 × 200 mm and the beta = 0.71. Therefore, the Faltin-type is preferred to the slot-ring structure and will be considered for application to the HIAF stochastic cooling system with the highest priority.

2) Beam Measurement for the Slot-Ring: To test the initial designs and accuracy of the HFSS, prototypes of the pickup with a total slot-ring length of 0.216 m, including 16 cells, were developed and tested on the HIRFL-CSR. A ceramic vacuum chamber (99% Al_2O_3 contains trace amounts of SiO_2 and MgO) was procured by Kunshan GuoLi Electronic in Soochow using the isostatic pressing method, with an inner diameter of 200 mm and a length of 250 mm. The ceramic material at both ends was brazed to the flange through a Kovar alloy transition. To release the static charge, the internal surface of the ceramic chamber, coated with around 1–10-nm Ti, eventually led to a sheet resistance per unit square value ranging from 10 to 100 kΩ/square, with the higher values preferred due to the virtual absence of RF attenuation. The slot-ring structure was manufactured in halves and then combined to form a whole ring. Fig. 20 shows a photograph of the 16 slot-ring cell structure, with a 16-way Wilkinson stripline-type combiner and an 8-mm thickness ceramic vacuum chamber. The longitudinal pickup shunt impedance measurement set-up for the slot-ring structure is shown in Fig. 21. The pickup shunt impedance of the 16 slot-ring cells is calculated according to (10), based on beam measurements. Fig. 22 shows a comparison of the pickup shunt impedance between the simulation result from the HFSS and the beam measurement using a $^{86}Kr^{30+}$ beam with energies of 476 and 268 MeV/u. Fig. 22 shows that the pickup shunt impedance values suddenly decreased from 0.81 to 0.87 GHz, which was largely because there were some interference signal probably from cell phone signal or military radar station and partly because alumina had 1% impurities, which could enhance adsorption and absorption of water vapor from the air, and partly because the impedance mismatch from feedthroughs and adapter of cables which are not considered in the simulation.

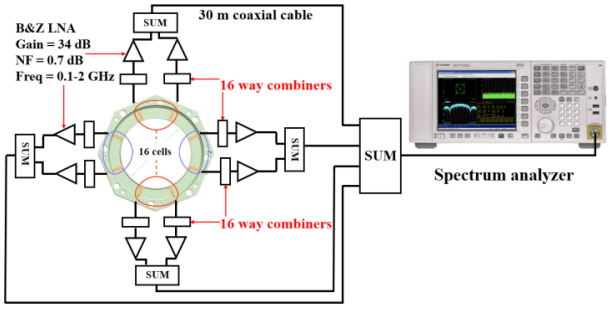

Fig. 21. Diagram of longitudinal shunt impedance measurement for 16 slot-ring cells with an 8-mm thickness ceramic vacuum chamber, where eight low noise amplifiers and eight 16-way Wilkinson stripline-type combiners were installed in the air.

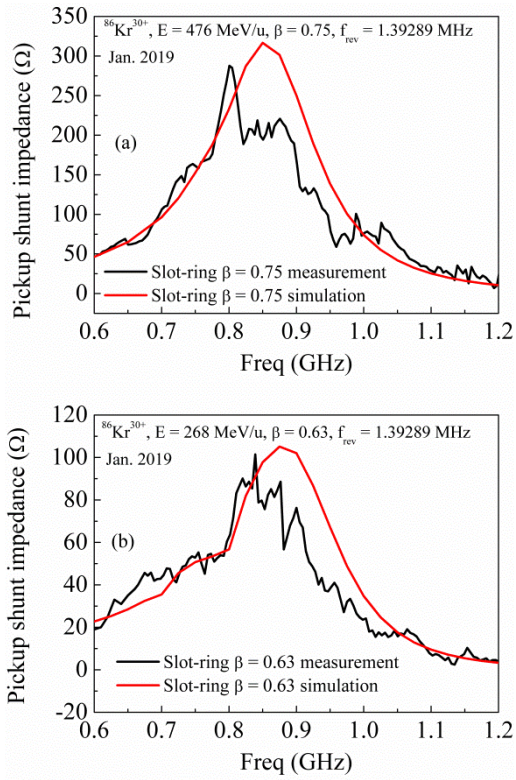

Fig. 22. Comparison of the slot-ring longitudinal pickup shunt impedance obtained with simulation and beam measurement: (a) energy = 476 MeV/u and (b) energy = 268 MeV/u. The particle number is approximately 5×10^7. It is normalized to 0.75 m in order to compare with Faltin structure.

This was the first time that a slot-ring installed outside the ceramic vacuum chamber as the pickup/kicker achieved a beam measurement. The advantages of the ceramic vacuum chamber being introduced into the slot-ring structure are that the shunt impedance improves by more than two times for beta = 0.83 and five times for beta = 0.71. Feedthroughs are avoided in a vacuum. It is easier to remove heat as a kicker when the combiner/divider board is in air rather than in a vacuum. It can be used for ultrahigh vacuum conditions requiring a 250°–300° high-temperature bake-out, which is one of our motivations to develop the slot-ring with a ceramic vacuum chamber. It is much easier to install and maintain when the slot-ring and combiner/divider board are in the air.

TABLE III
PARAMETERS USED IN THE SIMULATION OF SRING STOCHASTIC COOLING

Parameters	Numerical values
Beam	$^{132}Sn^{50+}$
Energy	400, 740 MeV/u
Particle number	1.0×10^5, 1.0×10^8
Initial momentum $\Delta p/p$	$\pm 4.0 \times 10^{-3}$
SRing circumference	277.3 m
Number of slot rings for pickup	64 cells
Number of slot rings for kicker	128 cells
Number of Faltin pickup (0.75 m)	2
Number of Faltin kicker (0.75 m)	4
Temperature (physical)	300 K
Bandwidth	600–1200 MHz
γ_t	3.317
Local γ_t	2.568
Dispersion at pickup/kicker	0 m

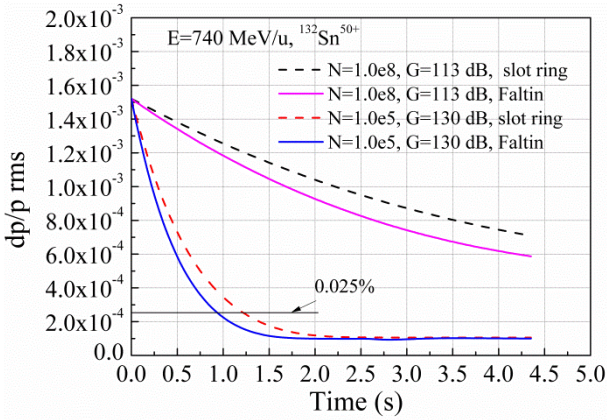

Fig. 23. Longitudinal momentum cooling and comparison of cooling times between the Faltin and slot-ring structures for a $^{132}Sn^{50+}$ beam with a beam energy of 740 MeV/u.

In addition, introducing the ceramic chamber into the slot-ring structure could reduce the manufacturing costs, reduce the associated difficulties, and shorten the production cycle.

IV. SIMULATION CALCULATIONS OF THE COOLING PROCESS

According to the shunt impedance results for the Faltin and slot-ring structures, we simulated the longitudinal cooling processing and RF power requirement using C programming language in Microsoft Visual Studio 2015 [23] for the SRing stochastic cooling system through the Fokker–Planck equation [24], [25]. This numerical method has been verified in [6]. In HIAF phase I project, stochastic cooling will be mainly applied to fresh secondary beams experiment, and the particle number will be less than 1×10^5. The parameters used in the simulation of the SRing stochastic cooling are shown in Table III. For high charge-state beams, with a small particle number of 1.0×10^5, for example, $^{132}Sn^{50+}$, the cooling speed is sufficient with a gain of 130 dB, as shown in Figs. 23 and 24, which means that the noise power is less than 100 W, as shown in Table IV. To account for losses in the cooling chain and for

TABLE IV
RF POWER REQUIREMENT FOR A $^{132}Sn^{50+}$ BEAM MOMENTUM COOLING SIMULATIONS IN THE BANDWIDTH 0.6–1.2 GHz

Energy (MeV/u)	Particle Numbers	Gain (dB)	Type of Structure	RF Power (W)
400	1×10^5	130	Slot ring	50
			Faltin	60
	1×10^8	113	Slot ring	130
			Faltin	290
740	1×10^5	130	Slot ring	50
			Faltin	55
	1×10^8	113	Slot ring	300
			Faltin	370

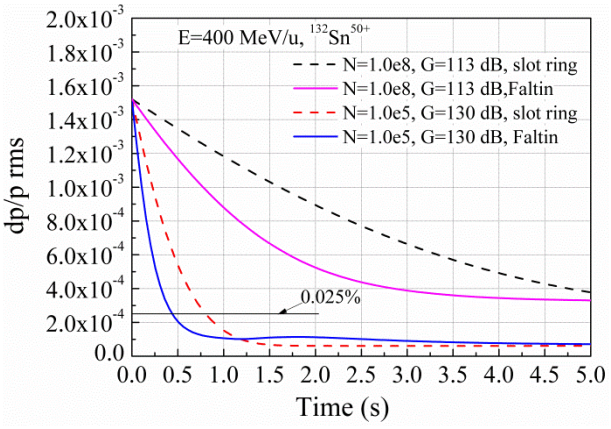

Fig. 24. Longitudinal momentum cooling and comparison of the cooling times between the Faltin and slot-ring structures for a $^{132}Sn^{50+}$ beam with a beam energy of 400 MeV/u.

the statistical nature of the cooling signals, a safety factor of 4–6 has to be included to avoid signal distortions due to amplifier nonlinearities, and therefore, the necessary electronic power is 4–6 times the noise power [25]. This guarantees that the amplifiers are not saturated and no additional heating is introduced. Figs. 23 and 24 also show that the cooling time using the Faltin structure as a pickup/kicker is less than that using the slot-ring structure.

V. CONCLUSION

The development, performance, and testing of both a Faltin prototype traveling wave structure and a novel slot-ring prototype standing wave structure based on a ceramic vacuum chamber for the HIAF SRing stochastic cooling system are presented in this article. This article introduces in detail and systematically describes how to design a Faltin-type and slot-ring-type pickup/kicker using the HFSS software. This HFSS simulation method is very efficient and can be used to design and develop other pickup/kicker structures, especially for the standing wave structure. In the simulation, it is shown that the optimized shunt impedance of both Faltin-type and slot-ring-type pickup/kicker can cover the energy range from 400 MeV/u ($\beta = 0.71$) to 740 MeV/u ($\beta = 0.83$) in the bandwidth 0.6–1.2 GHz. Also, we observe that if the slot-ring structure is installed outside a ceramic vacuum chamber, the kicker shunt impedance can be significantly improved.

The first time that a slot-ring structure installed outside the ceramic vacuum chamber as the pickup/kicker and achieved a beam measurement was at the end of 2018. Pickup shunt impedance measurements for both the Faltin and slot-ring prototypes were found to agree well with the results of HFSS simulations, indicating that the simulation results are reliable. In HIAF phase I project, since the beam aperture size of the SRing is 120 × 200 mm and the beam energy was 400 MeV/u (beta = 0.71), the maximum optimized longitudinal kicker shunt impedance of the 0.75 m slot-ring structure for beta = 0.71 was 950 Ω at 0.85 GHz, which is smaller than the value for Faltin structure of 1349 Ω at 1.197 GHz. In addition, Faltin-type have the advantage of low number of feedthroughs, robustness, low manufacturing cost and ease of manufacture. Therefore, we select the Faltin structure as the pickup and the kicker of the SRing stochastic cooling system at present. The design stage of the Faltin-type pickup/kicker beam devices has been completed for the SRing stochastic cooling system and is now entering the fabrication and testing stage.

However, in the future HIAF phase II upgrade project, the energy of the stochastic cooling system will reach 740 MeV/u (beta = 0.83) and the beam pipe diameter of the SRing will be 118 mm. The one cell slot-ring shunt impedance will reach 53 Ω at 0.95 GHz, as shown in Fig. 17(a), then the maximum longitudinal kicker shunt impedance of the 0.75 m (55 cells) slot-ring structure for beta = 0.83 will be 2915 Ω, which will much larger than the value for Faltin structure of 1349 Ω at 1.197 GHz, as shown in Fig. 7(a). Therefore, the slot-ring structure installed outside the ceramic vacuum chamber as the pickup/kicker will be considered for application to the future HIAF phase II upgrade project with the highest priority.

In the next beam experiment, we will continue to study the slot-ring-type based on a ceramic vacuum chamber by shielding interference signals and control the humidity of the ceramic tube and so on. This structure is very competitive for small beam pipe size and high energy machine. It will also be useful for some other stochastic cooling facilities.

ACKNOWLEDGMENT

The authors would like to thank Lars Thorndahl (CERN), Fritz Nolden [GSI Helmholtzzentrum für Schwerionenforschung GmbH (GSI)], Bernd Breitkreutz (Jülich), Rolf Stassen (Jülich), Takeshi Katayama, and

Vladimir Dragon [Joint Institute for Nuclear Research (JINR)] who have provided strong support for many years. They would also like to thank the editor and the anonymous reviewers of the journal for their constructive remarks and helpful suggestions which improve the quality of this article.

REFERENCES

[1] X. W. Ma *et al.*, "HIAF: New opportunities for atomic physics with highly charged heavy ions," *Nucl. Instrum. Meth. Phys. Res. B, Beam Interact. Mater. At.*, vol. 408, pp. 169–173, Mar. 2017.

[2] J. C. Yang *et al.*, "High intensity heavy ion accelerator facility (HIAF) in China," *Nucl. Instrum. Meth. Phys. Res. Sect. B, Beam Interact. with Mater. At.*, vol. 317, pp. 263–265, Dec. 2013.

[3] B. Wu *et al.*, "The design of the spectrometer ring at the HIAF," *Nucl. Instrum. Meth. Phys. Res. A, Accel. Spectrom. Detect. Assoc. Equip.*, vol. 881, pp. 27–35, Feb. 2018.

[4] S. Chattopadhyay, "On stochastic cooling of bunched beams from fluctuation and kinetic theory," Ph.D. dissertation, Dept. Accel. Fusion Res. Division, Univ. California Berkeley, Berkeley, CA, USA, 1982.

[5] F. Nolden *et al.*, "The collector ring CR of the FAIR project," in *Proc. 10th Eur. Part. Accel. Conf.*, Edinburgh, Scotland, 2006, pp. 1–5. [Online]. Available: http:// accelconf.web.cern.ch/

[6] G. Y. Zhu *et al.*, "Stochastic cooling experiments for CSRe at IMP," *Nucl. Instrum. Meth. Phys. Res. A, Accel. Spectrom. Detect. Assoc. Equip.*, vol. 932, pp. 83–89, Jul. 2019.

[7] W. Kells, "Filterless fast momentum cooling," in *Proc. 11th Int. Conf. High-Energy Accel.*, Geneva, Switzerland, Jul. 1980, p. 777.

[8] G. Carron and L. Thorndahl, "Stochastic cooling of momentum spread with filter techniques," *CERN/ISR-RF*, vol. 78, no. 12, p. 15, 2015.

[9] F. Voelker *et al.*, "An array of 1-2 GHz electrodes for stochastic cooling," in *Proc. IEEE Conf. Nucl. Sci.*, 1983, p. 2262.

[10] G. Lambertson *et al.*, "Measurement of frequency response of LBL stochastic cooling arrays for TeV-1 storage rings," in *Proc. PAC IEEE Conf.*, Vancouver, BC, Canada, 32 1985, p. 2168.

[11] B. Autin, G. Carron, F. Caspers, S. Milner, L. Thorndahl, and S. van der Meer, "ACOL stochastic cooling systems," in *Proc. PAC*, Washington, DC, USA, 1987, pp. 1–5.

[12] S. Baird *et al.*, "Design study of the antiproton delelerator: AD," CERN, Meyrin, Switzerland, Tech. Rep. CERN/PS 96-43 (AR), 1996.

[13] P. Brittner *et al.*, "The stochastic-cooling system for COSY-julich," in *Proc. Conf. Rec. IEEE Part. Accel. Conf.*, 1425, p. 1425.

[14] F. Nolden, C. Dimopoulou, A. Dolinskii, and M. Steck, "Storage rings for radioactive ion beams," *Nucl. Instrum. Meth. Phys. Res. Sect. B, Beam Interact. with Mater. At.*, vol. 266, nos. 19–20, pp. 4569–4574, Oct. 2008.

[15] D. Möhl, *Stochastic Cooling of Particle Beams* (Lecture Notes in Physics), vol. 866. Berlin, Germany: Springer, 2013. [Online]. Available: https://link.springer.com/book/10.1007/978-3-642-34979-9

[16] D. A. Goldberg and G. R. Lambertson, "Dynamic devices: A primer on pickups and kickers," *Amer. Inst. Phys.*, vol. 2008, p. 542, Dec. 2008.

[17] D. A. Goldberg and G. R. Lambertson, "Dynamic devices: A primer on pickups and kickers," in *Proc. Amer. Inst. Phys.*, 2008, pp. 555–559.

[18] ANSYS HFSS High Frequency Structure Simulator, Canonsburg, PA, USA. (2016). [Online]. Available: http://www.ansys.com/

[19] L. Faltin, "Slot-type pick-up and kicker for stochastic beam cooling," *Nucl. Instrum. Meth.*, vol. 148, no. 3, pp. 449–455, Feb. 1978.

[20] J. W. Xia *et al.*, "The heavy ion cooler-storage-ring project (HIRFL-CSR) at lanzhou," *Nucl. Instrum. Meth. Phys. Res. A, Accel. Spectrom. Detect. Assoc. Equip.*, vol. 488, nos. 1–2, pp. 11–25, Aug. 2002.

[21] R. Stassen, P. Brittner, R. Greven, H. Singer, H. Stockhorst, and L. Thorndahl, "Recent developments for the HESR stochastic cooling system," *Proc. COOL*, Bad Kreuznach, Germany, 2007, p. 9.

[22] E. brambilla-Innocente, "A microwave Cerenkov pick-up for stochastic cooling," *CERN*, vol. 45, p. 15, Oct. 1985.

[23] Microsoft Visual Studio, Redmond, WA, USA. (2015). [Online]. Available: https://visualstudio.microsoft.com/

[24] L. Thorndahl, "Diffusion in momentum space caused by filtered noise," CERN, Meyrin, Switzerland, Internal Rep. CERN/ISR-RF-TH, Aug. 1977, vol. 19.

[25] H. Stockhorst, T. Katayama, and R. Maier, "Beam cooling at COSY and HESR," Schriften des Forschungszentrums Jülich, Jülich, Germany, Tech. Rep., 2016. [Online]. Available: https://juser.fz-juelich.de/record/807739